CHEMISTRY
A EUROPEAN JOURNAL

DOI: 10.1002/chem.201102330

Combustion Synthesis and Electrochemical Properties of the Small Hydrofullerene $C_{50}H_{10}$

Jian-Hua Chen,[a, b] Zhi-Yong Gao,[a, c] Qun-Hong Weng,[a] Wen-Sheng Jiang,[a] Qiao He,[a] Hua Liang,[a, d] Lin-Long Deng,[a] Su-Lan Xie,[a] Hui-Ying Huang,[e] Xin Lu,[a] Su-Yuan Xie,*[a] Kang Shi,*[a] Rong-Bin Huang,[a] and Lan-Sun Zheng[a]

Abstract: The hydrofullerene $C_{50}H_{10}$ is synthesized by low-pressure benzene–oxygen diffusion combustion. The structure of $C_{50}H_{10}$ is identified through NMR, mass spectrometry, and IR and Raman spectroscopy as a D_{5h} symmetric closed-cage molecule with five pairs of fused pentagons stabilized by ten hydrogen atoms. UV/Vis and fluorescence spectrometric analyses disclose its optical properties as comparable with those of its chloride cousin ($C_{50}Cl_{10}$). Cyclic and square-wave voltammograms reveal that the first reduction potential of $C_{50}H_{10}$ is more negative than that of $C_{50}Cl_{10}$ as well as C_{60}, with implications for the utilization of $C_{50}H_{10}$ as a promising electron acceptor for photovoltaic applications.

Keywords: combustion · electrochemistry · fullerenes · NMR spectroscopy · Raman spectroscopy · solar cells

Introduction

Fullerenes smaller than C_{60}, unavoidably defying the isolated pentagon rule (IPR),[1] have been theoretically predicted to render special properties.[2] However, only a few smaller fullerenes have been synthesized, typically stabilized as halogenated fullerenes such as $^{\#271}C_{50}Cl_{10}$,[3] (numbered according to the Fowler–Manolopoulos spiral codes[4]), $^{\#540}C_{54}Cl_8$,[5] $^{\#864}C_{56}Cl_{12}$,[5] $^{\#913}C_{56}Cl_{10}$,[6] $^{\#916}C_{56}Cl_{10}$[7] and the heptagon-incorporating $C_{58}F_{18}$.[8]

[a] Dr. J.-H. Chen, Dr. Z.-Y. Gao, Q.-H. Weng, W.-S. Jiang, Q. He, Dr. H. Liang, L.-L. Deng, S.-L. Xie, Prof. X. Lu, Prof. S.-Y. Xie, Prof. K. Shi, Prof. R.-B. Huang, Prof. L.-S. Zheng
State Key Lab for Physical Chemistry
of Solid Surfaces & Department of Chemistry
College of Chemistry and Chemical Engineering
Xiamen University, Xiamen 361005 (China)
Fax: (+86) 592-2183047
E-mail: syxie@xmu.edu.cn
kshi@xmu.edu.cn

[b] Dr. J.-H. Chen
Current address: Yunnan Academy of Tobacco Science
R&D Center for Safety Evaluation of Tobacco Additives, Kunming, China.

[c] Dr. Z.-Y. Gao
Current address: School of Chemistry and Environmental Science
Henan Normal University, Xinxiang, China.

[d] Dr. H. Liang
Current address: State Key Lab of Cultivation Base for
Non-metal Composites & Functional Materials
Southwest University of Science and Technology, Mianyang, China.

[e] Dr. H.-Y. Huang
School of Life Science, Xiamen University
Xiamen 361005 (China)

Supporting information for this article is available on the WWW under http://dx.doi.org/10.1002/chem.201102330.

Among these, C_{50} (referring to #271 if there is no specific notation) is the representative one with the smallest fullerene core without triple pentagons directly or sequentially fused.[9] C_{50} is also one of the predominant magic clusters originally produced in the gas phase.[10]

Since the experimental availability of $C_{50}Cl_{10}$ in the arc-discharge of graphite,[3] attention has been paid to its properties and reactions. For example, the electronic properties of C_{50} and its derivatives were studied using density functional theory.[11a,b] The stable isomers of C_{50} were geometrically optimized by entropy contributions in addition to the B3LYP/631G* method.[11c] The X-ray photoelectron, ultraviolet photoelectron, and near-edge X-ray absorption spectra for the $C_{50}Cl_{10}$ molecule were simulated theoretically.[11d] The electrostatic potential distributions were calculated in order to facilitate the understanding of C_{50} derivatization such as protonation and alkylation.[11e] In addition, the 1,3-dipolar cycloaddition[12a] and Diels–Alder cycloaddition[12b] reactions were considered for C_{50}. The stabilities of $C_{50}Cl_{10}$ solid[13a] and C_{50} derivatives $C_{50}O$,[13b] $C_{50}X$ ($X=CH_2$, NH, SiH_2, PH, S),[13c,d] and $C_{50}X_2$ ($X=H$, F, Cl, Br, OH)[13e] were studied theoretically. The endohedral complexes $X@C_{50}$ ($X=H$, Li, Na, K, Be, Mg, Ca) were also computed using the B3LYP/6-31G method.[14] However, the properties of fullerenes smaller than C_{60} remain to be explored experimentally.

As one of the most remarkable properties of fullerenes, their electrochemical behaviors have been widely studied.[15] Their outstanding redox properties make fullerenes and their derivatives useful as electron-accepting materials. For example, some derivatives of C_{60}, C_{70}, and $Lu_3N@C_{80}$ have been used as promising *n*-type materials in organic solar-cell devices.[16] On the basis of the experimental accessibility of D_{5h}-symmetric C_{50} chloride, we have also paid special atten-

tion to the electrochemical properties of $C_{50}Cl_{10}$ in recent years. However, the reduced products, $C_{50}Cl_{10}^{n-}$ ($n=1, 2 \ldots$), are too reactive to serve as electron acceptors. We thus turned our attention to the hydrogenated derivatives, e.g., $C_{50}H_{10}$. Various theoretical studies had been carried out previously for the hydrides of C_{50} by pioneers soon after the macroscopic synthesis of C_{60} and C_{70}.[13c,17] However, efforts to synthesize $C_{50}H_{10}$ experimentally was fruitless. Here we report a combustion synthesis of $C_{50}H_{10}$, and a validation of the structural prediction originally proposed by Kroto two decades ago.[17a] The Saturn-like structure with D_{5h} symmetry and optical properties comparable to those of $C_{50}Cl_{10}$ have been established by spectrometric identifications. Remarkably, cyclic voltammetric analysis reveals that the newly synthesized hydride, in contrast to $C_{50}Cl_{10}$, exhibits reversible redox behavior occurring at more negative potentials with possible application in photovoltaic devices.

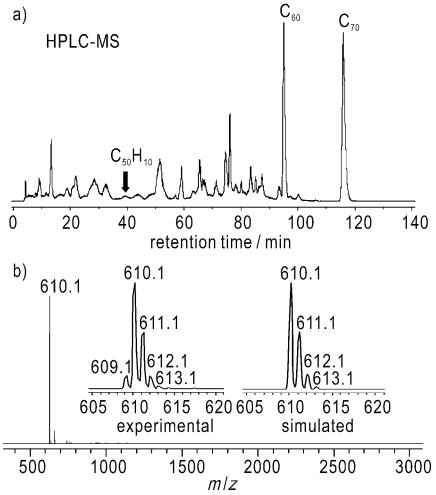

Figure 2. a) HPLC-MS chromatogram of the toluene-extracted soot products. b) Mass spectrum of the purified $C_{50}H_{10}$. The insets show the experimental and simulated mass spectra of $C_{50}H_{10}$.

Results and Discussion

Synthesis of $C_{50}H_{10}$ in flame: The $C_{50}H_{10}$-containing soot was synthesized in our homemade setup with a diffusion flame of benzene–oxygen.[18a] The flame was maintained under a pressure of 10–20 torr in the homemade setup, the burner of which consisted of two concentric tubes with the same center. Oxygen was fed in the inner tube, while benzene flowed through the space between the two concentric tubes. In contrast to the classical arc-discharge method,[19] the combustion method is more viable for the macroscopic and continuous synthesis that is critical for application on an industrial scale.[20] Very recently, we developed the benzene–oxygen flame for the synthesis of IPR-violating fullerenes such as $^{\#1911}C_{64}H_4$ and $^{\#1809}C_{60}H_8$.[18] In the combustion process, both the amount of soot and the yield of fullerene are very sensitive to the C/O ratio of the reactants. As shown in Figure 1, an increase in the C/O molar ratio leads to a decrease in the C_{60} and C_{70} yields, but the total amount of soot increases. The C/O ratio was optimized at ≈ 1 in the present experiment.

Structural characterization of $C_{50}H_{10}$: Figure 2a shows the HPLC-MS chromatogram of a toluene solution extracted from the combustion soot (see the Supporting Information for the HPLC analysis conditions in detail). The chromatogram is dominated by C_{60} and C_{70}, together with a minor component of $C_{50}H_{10}$ and other hydrocarbons. The mass spectrum of the purified sample of $C_{50}H_{10}$ is shown in Figure 2b, which shows a molecular ion peak of 610.1 m/z, in agreement with the chemical composition of $C_{50}H_{10}$. However, the purified $C_{50}H_{10}$ is subject to oxidization in air. Stored in a toluene solution (without removal of air) for a few months, the oxides of $C_{50}H_{10}$ increased markedly (see the Supporting Information).

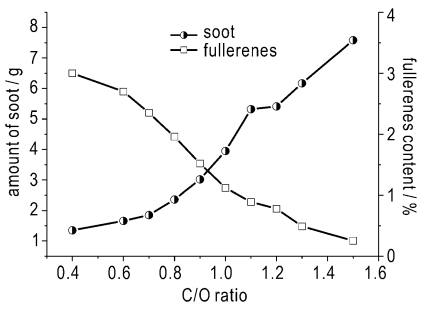

Figure 1. Curves of the amount of soot and the yield of fullerenes (C_{60} plus C_{70}) as a function of the C/O ratio.

The structure and molecular symmetry of $C_{50}H_{10}$ were characterized by means of NMR spectroscopy on a Bruker AV 600 MHz spectrometer. Figure 3a shows the ^{13}C NMR spectrum of $C_{50}H_{10}$ in $CDCl_3$. The three peaks located at 161.8, 150.2, and 145.4 ppm are characteristic of three types of sp^2-hybridized carbon atoms, and the peak located at 55.0 ppm is typical of sp^3-hybridized carbon atoms. Among 271 possible cage structures in the C_{50} isomer family, only the D_{5h} symmetric isomer with five pairs of adjacent pentagons has four unique types of carbon atoms. Almost certainly, the hydrogen atoms are attached to each of the ten carbon atoms at the fusions of the adjacent pentagons (Figure 3d). The structure of $C_{50}H_{10}$ was further characterized by its ^1H NMR spectrum (Figure 3b), which showed one dominant signal (at 5.35 ppm) without ^1H-^1H coupling. These NMR signals are analogous to those of $C_{50}Cl_{10}$ (Figure 3c), the geometric structure of which has recently been confirmed by single-crystal X-ray diffraction.[21] For $C_{50}Cl_{10}$, the ^{13}C NMR spectrum also contains four distinct signals located at 161.5 (C_I), 146.6 (C_{II}), 143.0 (C_{III}), and 88.7 (C_{IV}) ppm.[3] The first three NMR signals (at the C_{I-III} sites) are comparable in chemical shift, but the last one (C_{IV}) is shifted upfield by ≈ 33.7 ppm for $C_{50}H_{10}$. This is probably due to the chlorine atom being a stronger electron-withdrawing group. On the other hand, the ^{13}C NMR signal intensity of the sp^3-

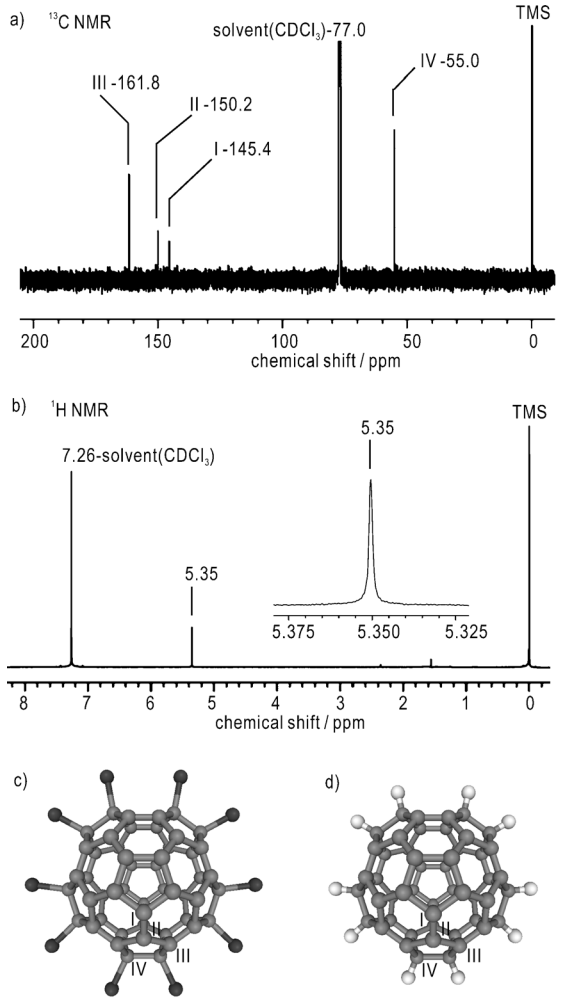

Figure 3. a) ^{13}C NMR spectrum of $C_{50}H_{10}$ (150 MHz, $CDCl_3$ solvent, room temperature). b) ^{1}H NMR spectrum (600 MHz, $CDCl_3$ solvent, room temperature). The inset shows the amplified signal around 5.35 ppm. c) Molecular structure of $C_{50}Cl_{10}$. d) Molecular structure of $C_{50}H_{10}$.

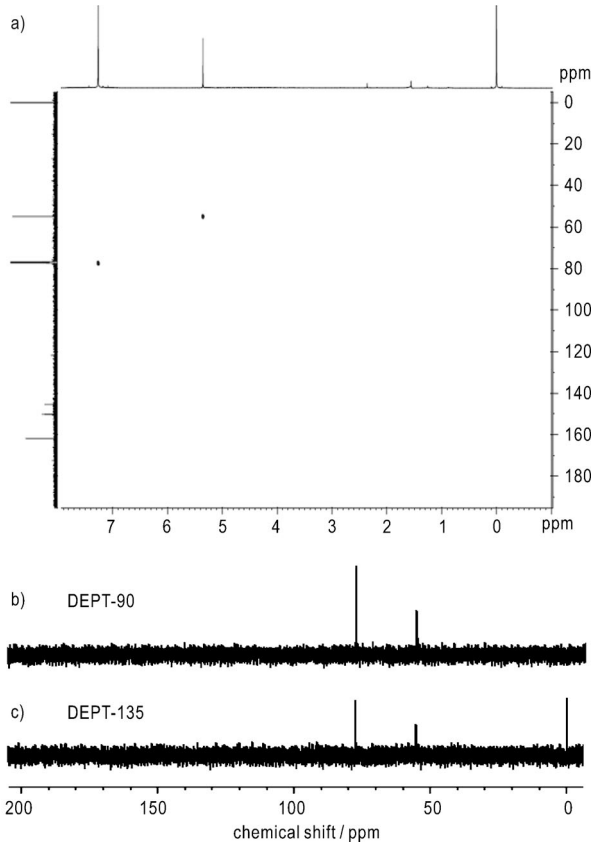

Figure 4. a) ^{1}H, ^{13}C HSQC spectrum of $C_{50}H_{10}$; the circle indicates the correlativity of the C_{IV} carbon and hydrogen. b) DEPT 90 spectrum. c) DEPT 135 spectrum. The ^{13}C signal at 77.0 is due to chloroform.

hybridized carbon atoms of $C_{50}Cl_{10}$ is much weaker than that of $C_{50}H_{10}$. Such a stronger NMR signal of the sp^3-hybridized carbon atoms in the hydride implies a significant coupling effect between the C and H nuclei in $C_{50}H_{10}$.

Two-dimensional Heteronuclear Single Quantum Coherence (2D HSQC) NMR measurements were performed to further confirm the connectivity between the sp^3-hybridized carbon atoms and the ten hydrogen atoms (Figure 4a). Only the C_{IV} carbon atoms ($\delta = 55.0$ ppm) at the fusions of the fused pentagons show correlations with the hydrogen atoms. Moreover, the Distortionless Enhancement by Polarization Transfer (DEPT) 90 and DEPT 135 spectra indicate that all the sp^3-hybridized carbon atoms are tertiary carbon atoms in the carbon cage framework (Figures 4b and 4c). Therefore, it can be concluded that the structure of $C_{50}H_{10}$ is a D_{5h} symmetric carbon cage with five pairs of fused pentagons to which ten hydrogen atoms are attached (Figure 3d).

In addition, the molecule of $C_{50}H_{10}$ was characterized by FTIR and Raman spectroscopy in comparison to $C_{50}Cl_{10}$. The IR spectra shown in Figure 5 were recorded on a Nicolet 380 Fourier-transform infrared instrument, using a KBr disc coated with a $C_{50}H_{10}$ or $C_{50}Cl_{10}$ solid film. The absorption at ≈ 2900 cm^{-1} in the spectrum of $C_{50}H_{10}$ is ascribed to the C–H stretching mode, and the absorption at ≈ 854 cm^{-1} is assignable to C–Cl stretching in the spectrum of $C_{50}Cl_{10}$ but not in that of $C_{50}H_{10}$. As shown in Figure 6, the vibrational differentiations are also observed in the Raman spectra. The featured signals at ≈ 912–987 cm^{-1} can be assigned to the C–Cl mode, whereas the signals at 554 and 520 cm^{-1} are due to the C–H mode (see the Supporting Information).

Optical spectroscopic analysis of $C_{50}H_{10}$ compared to $C_{50}Cl_{10}$: Figure 7a shows the UV/Vis absorption spectrum of $C_{50}H_{10}$ in cyclohexane. The major absorptions of $C_{50}H_{10}$ are located at 210, 238, 268, 315, 350, 380, and 435 nm, in good agreement with the calculated results.[11b] According to calculations at the TD-BP86/3-21G level, the first singlet excitation (mainly HOMO to LUMO) of $C_{50}H_{10}$ is optically forbidden at 490.2 nm (2.53 eV), which is blue-shifted by ≈ 100 nm compared with the first singlet excitations of $C_{50}Cl_{10}$. The UV/Vis spectrum of $C_{50}Cl_{10}$ is shown in Figure 7b for comparison.

The emission fluorescence spectra of both $C_{50}H_{10}$ and $C_{50}Cl_{10}$ in cyclohexane are shown in Figure 8. Although the

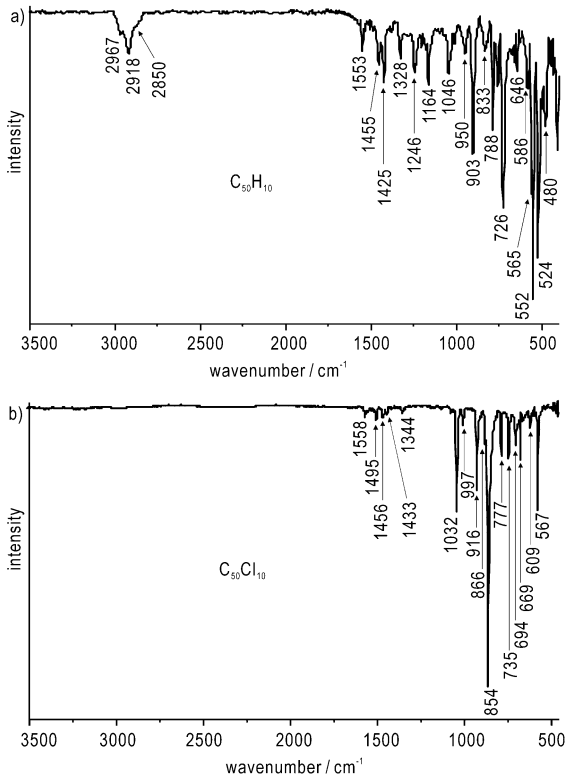

Figure 5. IR spectra of a) $C_{50}H_{10}$ and b) $C_{50}Cl_{10}$.

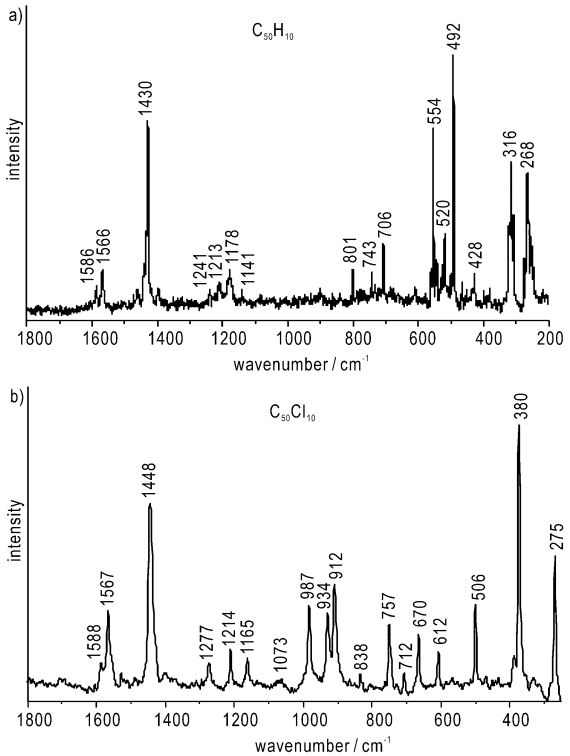

Figure 6. Raman spectra of a) $C_{50}H_{10}$ and b) $C_{50}Cl_{10}$.

profiles with four peaks are similar for both compounds, the frequency data are totally different. The spectrum of $C_{50}H_{10}$

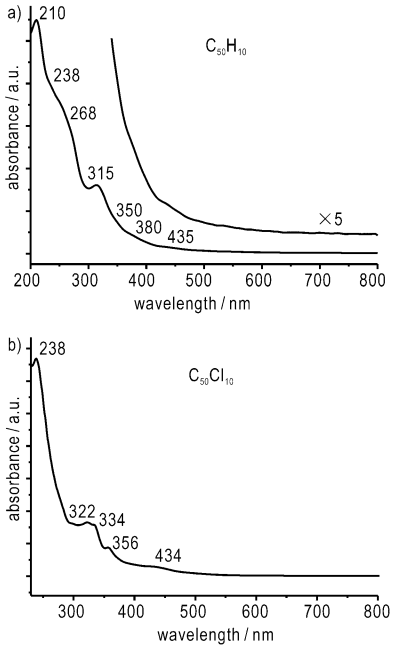

Figure 7. UV/Vis spectra of a) $C_{50}H_{10}$ and b) $C_{50}Cl_{10}$ in cyclohexane solution.

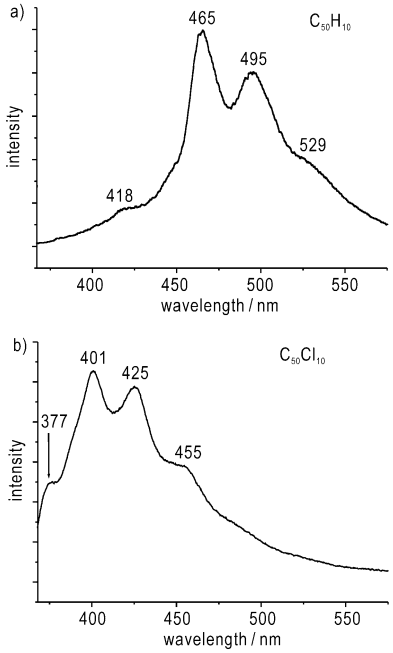

Figure 8. Fluorescence spectra of a) $C_{50}H_{10}$ and b) $C_{50}Cl_{10}$.

is well structured with four peaks at 418, 465, 495, and 529 nm. By contrast, $C_{50}Cl_{10}$ exhibits fluorescence signals at 377, 401, 425, and 455 nm. The four fluorescence wavelengths of the chlorofullerene are blue-shifted by ≈40–70 nm. Such a tunable optical property in the smaller fullerene derivatives might lead to potential applications in optical fields.[11b]

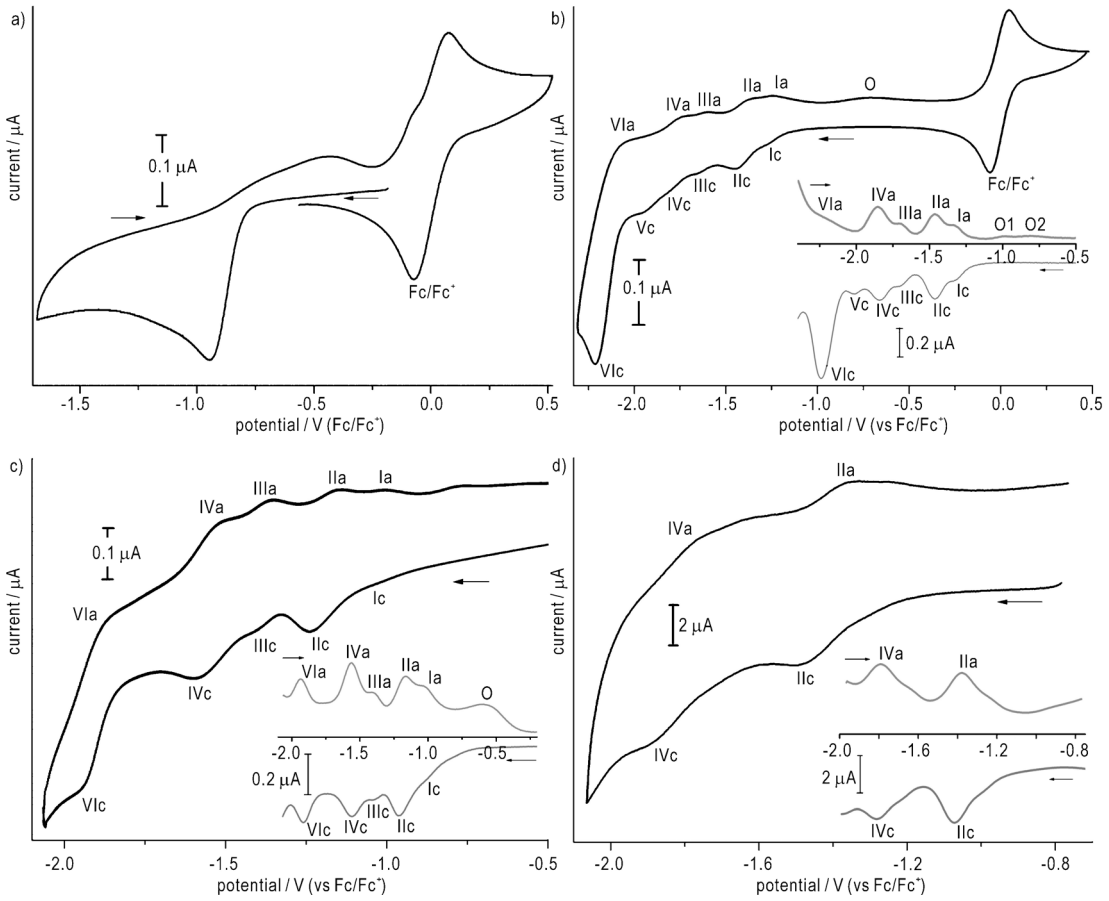

Figure 9. CVs of a) $C_{50}Cl_{10}$ and b) $C_{50}H_{10}$ on a Pt electrode (250 μm diameter) in a 0.05 M Bu_4NPF_6/ODCB solution at a scan rate of 0.05 V s^{-1}. c) CV of $C_{50}H_{10}$ solid coating on a Pt electrode (0.5 mm diameter) in a 0.1 M Bu_4NPF_6/acetonitrile solution at a scan rate of 0.05 V s^{-1}. d) CV of $C_{50}H_{10}$ on a Au electrode (2 mm diameter) in an acetonitrile/ODCB (1:5 vol/vol) mixture solution containing 0.1 M Bu_4NPF_6 at a scan rate of 4 V s^{-1}. The insets in (b), (c), and (d) are the OSWVs conducted with 4 mV increments (b, c) 25 mV amplitude and 25 Hz frequency; d) 50 mV amplitude and 50 Hz frequency]. The arrows indicate the scan directions.

Electrochemical properties of $C_{50}H_{10}$: The electrochemical properties of the C_{50} derivatives were investigated by cyclic and square-wave voltammetry (see the Experimental Section). Figure 9a shows the cyclic voltammogram (CV) of $C_{50}Cl_{10}$ taken at a scan rate of 0.05 V s^{-1} on a Pt electrode in a solution of *o*-dichlorobenzene (ODCB) containing 0.05 M tetrabutylammonium hexafluorophosphate (Bu_4NPF_6). Note that all potential data are reported relevant to the redox couple Fc/Fc^+. The electrochemically irreversible properties of $C_{50}Cl_{10}$ are shown in the asymmetric CV peaks, with a large reduction peak at −0.95 V and three small oxidation peaks at −0.79, −0.43, and 0.09 V.

By contrast, reversible redox pairs are shown in the CV of $C_{50}H_{10}$ (Figure 9b). The Osteryoung square-wave voltammogram (OSWV) (inset in Figure 9b) clearly reveals four pairs of reversible redox peaks (with mirror-image symmetry between the cathodic and anodic peaks) located at −1.36 (I), −1.46 (II), −1.70 (III), and −1.84 (IV) V. The other two reduction peaks at more negative potentials (peaks Vc and VIc at −2.10 and −2.24 V, respectively) and the oxidation peaks at potentials above −1.0 V (peaks O1 and O2) are dissymmetric to (or lacking) their corresponding oxidation/reduction signals.

We pay special attention to the six redox peaks with potential differences of ≈100–260 mV between the neighboring peaks in both the CV and OSWV of $C_{50}H_{10}$. Such a potential difference shown, for example, in Figure 9b obviously contradicts the previously reported data involving fullerene cages.[15,22–24] It has been well demonstrated that the electrochemical reduction of a closed-cage fullerene species such as C_{60} or C_{70} displays a separation of ≈450±50 mV between two successive redox peaks.[15,22–24] Interestingly, the six redox pairs can be classified into two groups with a potential difference of ≈400 mV, i.e., the larger peaks of II, IV, and VI, and the smaller peaks of I, III, and V, as shown in the OSWV (e.g., the inset of Figure 9b). Accordingly, it is reasonable to assume that the former group with the larger peaks originates from the successive reactions of $C_{50}H_{10}$, and the other group with the smaller peaks is relevant to the low content of other C_{50} species (e.g., the $C_{50}H_{10}$ oxides produced in the toluene solution, as identified in the Supporting Information. Although several HPLC runs were conducted, we failed to eliminate the trace oxides for a clean CV).

Because of the peak suppression caused by the oxides, the electron-transfer number of an individual redox reaction is difficult to determine by the traditional potentiostatic electrolysis method.[25] Alternatively, the electron-transfer number for each redox reaction can be evaluated from the peak separation ($\Delta E = E_a - E_c$) between the anodic and cathodic peaks recorded at a low scan rate. It is well known that ΔE is an indication of the electron number (n) involved in the corresponding reversible redox reaction based on the equation $\Delta E = 56.5/n$.[25] The well-defined redox peak couple II in the CV profile (Figure 9b) gives a ΔE value of ≈ 57 mV, indicating a reversible one-electron transfer step. Furthermore, the reversible redox peaks of II and IV display the equivalent peak heights in the OSWV profile (inset of Figure 9b), suggesting two successive redox reactions, each involving one electron, similar to those typically reported for C_{60} or C_{70}.[15]

However, the redox reaction relative to peak VI occurs irreversibly in the ODCB solvent (Figure 9b). We suppose the electrodes and working solution may be factors influencing the electrochemical response of $C_{50}H_{10}$. The CV and OSWV experiments with the $C_{50}H_{10}$-coated electrode were thus designed to be conducted in a working solution of acetonitrile (rather than ODCB). Through the dropping-evaporation method, the $C_{50}H_{10}$ sample was coated on a Pt electrode as an ultrathin solid layer.[26] The immobilized solid layer of $C_{50}H_{10}$ was measured in a 0.1 M Bu_4NPF_6/acetonitrile solution in which the solid $C_{50}H_{10}$ sample was insoluble. Interestingly, as shown in both the CV and the OSWV profile (Figure 9c), three couples of reversible redox peaks (II, IV, VI) with a potential difference of ≈ 390 mV and approximately equivalent peak heights dominate the voltammograms. In contrast to the asymmetric peak VI in Figure 9b, obviously, the reversibility of peak VI can be observed through the replacement of ODCB by acetonitrile as the working solution and modification of the electrode with a coating of $C_{50}H_{10}$. The designed experiment also leads to the positive shift (≈ 300 mV) of all the reversible redox peaks, and to a decrease in the current of peak Vc. Presumably, such a solvent-dependent difference may be due partly to the electrocatalytic dehydrogenation of the $C_{50}H_{10}$ reduction product, similarly to those reported for other fullerenes.[27] A detailed insight into the mechanism is open for future study.

As electron acceptors, fullerenes have potential applications in organic solar cells, in which gold is traditionally used as the substrate electrode. It is thus important to know the electrochemical properties of $C_{50}H_{10}$ on metallic gold. Figure 9d shows a CV of $C_{50}H_{10}$ on a Au electrode in an acetonitrile/ODCB (1:5 vol/vol) solvent mixture at a fast scan rate of 4 $V s^{-1}$. $C_{50}H_{10}$ again displays two couples of reversible redox peaks II ($E_{pc} = -1.47$ V, $E_{pa} = -1.35$ V) and IV ($E_{pc} = -1.87$ V, $E_{pa} = -1.76$ V) within the potential range investigated. The $E_{1/2}$ values for these two redox processes are -1.41 and -1.82 V, respectively. These observations indicate that $C_{50}H_{10}$ is capable of exhibiting better chemical and electrochemical reversibility on the Au electrode, as the signals of small amounts of impurities (e.g., $C_{50}H_{10}O_n$) can be partially restrained.

Theoretical calculations assume a more positive reduction potential for higher fullerenes ($> C_{60}$), though the $E_{1/2}$ values for both C_{60} and C_{70} are approximately equal in the first reduction process in ODCB (-1.07 V versus Fc/Fc^+), tetrahydrofuran (-0.88 to -0.85 V versus Fc/Fc^+), dichloromethane (-0.92 to -0.97 V versus Fc/Fc^+), and benzonitrile (-0.91 V versus Fc/Fc^+).[22] The abnormal phenomenon of the approximately equal values of $E_{1/2}$ for both C_{60} and C_{70} has been interpreted in terms of strain relief and pyracylene-type electronic character.[22b] In the present case, the first reduction potential of $C_{50}H_{10}$ (-1.41 V versus Fc/Fc^+ in acetonitrile/ODCB) is about 0.34 V more negative than the corresponding value of C_{60} (-1.07 V versus Fc/Fc^+ in ODCB) as well as its hydride $C_{60}H_2$ (-1.05 V versus Fc/Fc^+ in acetonitrile/toluene, -1.02 V versus Fc/Fc^+ in DMF/toluene),[23,24] indicating a higher LUMO for $C_{50}H_{10}$. Considering that the HOMO–LUMO gap of $C_{50}H_{10}$ was calculated to be 2.53 eV,[11b] the HOMO and LUMO of $C_{50}H_{10}$ can be speculated to be -5.90 and -3.37 eV, respectively. Both the LUMO and HOMO–LUMO gap values of $C_{50}H_{10}$ are suitable for photovoltaic applications in, for example, poly(3-hexylthiophene-2,5-diyl) (P3HT)-fullerene bulk heterojunction solar cells. It is known that the open-circuit voltage (V_{oc}) of a fullerene-based organic solar cell depends heavily on the HOMO level of the polymer donor and the LUMO level of the fullerene acceptor. As a useful electron-acceptor material, the fullerene derivative of 1-(3-methoxycarbonyl) propyl-1-phenyl[6,6] C_{61} ($PC_{60}BM$) has been employed widely in P3HT:PC_nBM bulk heterojunction solar cells.[28] However, the LUMO of $PC_{60}BM$ is too low to prepare a P3HT:$PC_{60}BM$ bulk heterojunction solar cell with higher V_{oc}. Many other fullerene derivatives with higher LUMO levels (i.e., with more negative values for the first reduction potential) have been used to replace $PC_{60}BM$ in order to improve the efficiency of photovoltaic cells. For instance, by the replacement of C_{60} with $Lu_3N@C_{80}$ (having the first reduction potential at -1.42 V versus Fc/Fc^+ in ODCB), V_{oc} of P3HT:PC_nBM ($C_n = C_{60}$, $Lu_3N@C_{80}$) bulk heterojunction solar cells could be improved from 630 mV (for C_{60}) to 810 mV (for $Lu_3N@C_{80}$).[16b] Similarly, the higher LUMO level of $C_{50}H_{10}$ may lend credence to promising applications of $C_{50}H_{10}$ in fullerene-based solar cells. However, it should be envisaged that a realistic photovoltaic application depends on the macroscopic synthesis of the involved C_{50} material, the investigation of which is still underway at this stage.

Conclusion

In conclusion, the small hydrofullerene D_{5h}-$^{\#271}C_{50}H_{10}$ has been synthesized by low-pressure benzene–oxygen (with 1:1 C/O ratio) diffusion combustion flames, which can be operated in continuous fashion and can be expected to be useful for the large-scale production of various non-IPR fullerene

hydrides (e.g., $^{\#1809}C_{60}H_8$, $^{\#1911}C_{64}H_4$, and others). The symmetry and structure of $C_{50}H_{10}$ have been identified by ^1H and ^{13}C NMR measurements, as well as IR and Raman spectroscopy. The UV/Vis and fluorescence spectrometric studies for $C_{50}H_{10}$ showed comparable optical properties to the previously synthesized $C_{50}Cl_{10}$. Through cyclic and square-wave voltammetry, $C_{50}H_{10}$ has been demonstrated to have more negative reduction potentials and better redox reversibility than its chlorofullerene cousin. Such remarkable electrochemical properties render the small non-IPR $C_{50}H_{10}$ a useful electron-acceptor material for potential application in fullerene-based photovoltaic devices. In view of the material availability and the useful properties of $C_{50}H_{10}$, further studies involving smaller hydrofullerenes might be stimulated.

Experimental Section

The fullerene soot was synthesized by a low-pressure benzene–oxygen diffusion combustion method.[18,29] The procedures for fullerene production in our homemade setup have been described previously.[18a] The C/O ratio was optimized at 1:1 to produce the maximum amount of $C_{50}H_{10}$-containing soot under a pressure of 10–20 Torr. Benzene vapor was fed as both the carbon source and hydrogen source. Through the combustion of benzene (a total of 10 L), $C_{50}H_{10}$-containing soot (about 350 g) was collected from the reaction chamber and the filter downstream. The collected soot was extracted with toluene in a supersonic bath at room temperature, and then filtered through a 0.5 μm filter. The isolation and purification of $C_{50}H_{10}$ was achieved by multistage HPLC with three columns, i.e., a pyrenebutyric acid bonded silica column (i.d. 20 mm × 250 mm), a Buckyprep column (i.d. 20 mm × 250 mm, Cosmosil), and a 5PBB column (i.d. 20 mm × 250 mm, Cosmosil). Purified $C_{50}H_{10}$ (about 3 mg) was obtained. Figure S1 of the Supporting Information shows the detailed procedure for the separation and purification of $C_{50}H_{10}$ by multistage HPLC.

The mass spectra were determined on a Bruker Esquire HCT instrument with an atmospheric pressure chemical ionization (APCI) source in negative ion mode. The NMR spectra were acquired on a Bruker AV 600 MHz instrument with a Cryo-Probe system. The UV/Vis absorption and fluorescence spectra were measured using a Shimadzu UV 3150 and a HITACHI F-4500 spectrometer, respectively. The FTIR spectra were recorded on a Nicolet 380 Fourier-transform infrared spectrometer. The Raman spectra were acquired on an RM 1000 instrument (Renishaw Co.) excited by a laser of 785 nm.

All electrochemical measurements were performed using a CHI-660C analyzer (CH Instruments, Inc.) in a glove box at room temperature (20 ± 2 °C) under a nitrogen atmosphere. A conventional three-electrode cell was used, with a 250 or 500 μm diameter platinum or a 2 mm diameter gold wire (working electrode), a platinum foil (auxiliary electrode, 1 cm^2) and a platinum wire (pseudo-reference electrode). All potentials were reported versus the redox couple of the internal ferrocene/ferrocenium (Fc/Fc^+) standard. Before measurement, the working electrodes were polished with alumina slurry (0.3 μm), subsequently ultrasonicated in double-distilled water, and then dried in a nitrogen atmosphere.

Acknowledgements

Financial support was provided by the 973 projects (2011CB935901) and the NSFC (21031004, 21021061, 20773101).

[1] H. W. Kroto, *Nature* **1987**, *329*, 529–531.
[2] a) C. Piskoti, J. Yarger, A. Zettl, *Nature* **1998**, *393*, 771–774; b) P. G. Collins, J. C. Grossman, M. Cote, M. Ishigami, C. Piskoti, S. G. Louie, M. L. Cohen, A. Zettl, *Phys. Rev. Lett.* **1999**, *82*, 165–168; c) Z. F. Chen, H. J. Jiao, M. Bühl, A. Hirsch, W. Thiel, *Theor. Chem. Acc.* **2001**, *106*, 352–363; d) X. Lu, Z. F. Chen, *Chem. Rev.* **2005**, *105*, 3643–3696.
[3] S. Y. Xie, F. Gao, X. Lu, R. B. Huang, C. R. Wang, X. Zhang, M. L. Liu, S. L. Deng, L. S. Zheng, *Science* **2004**, *304*, 699.
[4] P. W. Fowler, D. E. Manoloupoulos, *An Atlas of Fullerenes*; Oxford University Press, Oxford, **1995**.
[5] Y. Z. Tan, J. Li, F. Zhu, X. Han, W. S. Jiang, R. B. Huang, Z. P. Zheng, Z. Z. Qian, R. T. Chen, Z. J. Liao, S. Y. Xie, X. Lu, L. S. Zheng, *Nat. Chem.* **2010**, *2*, 269–273.
[6] Y. Z. Tan, X. Han, X. Wu, Y. Y. Meng, F. Zhu, Z. Z. Qian, Z. J. Liao, M. H. Chen, X. Lu, S. Y. Xie, R. B. Huang, L. S. Zheng, *J. Am. Chem. Soc.* **2008**, *130*, 15240–15241.
[7] T. Zhou, Y. Z. Tan, G. J. Shan, X. M. Zou, C. L. Gao, X. Li, K. Li, R. B. Huang, L. S. Zheng, S. Y. Xie, *Chem. Eur. J.* **2011**, *17*, 8529–8532.
[8] P. A. Troshin, A. G. Avent, A. D. Darwish, N. Martsinovich, A. K. Abdul-Sada, J. M. Street, R. Taylor, *Science* **2005**, *309*, 278–281.
[9] T. G. Schmalz, W. A. Seitz, D. J. Klein, G. E. Hite, *J. Am. Chem. Soc.* **1988**, *110*, 1113–1127.
[10] H. W. Kroto, J. R. Heath, S. C. O'Brien, R. F. Curl, R. E. Smalley, *Nature* **1985**, *318*, 162–163.
[11] a) X. Lu, Z. F. Chen, W. Thiel, P. v. R. Schleyer, R. B. Huang, L. S. Zheng, *J. Am. Chem. Soc.* **2004**, *126*, 14871–14878; b) R. H. Xie, G. W. Bryant, C. F. Cheung, V. H. Smith, J. J. Zhao, *J. Chem. Phys.* **2004**, *121*, 2849–2851; c) X. Zhao, *J. Phys. Chem. B* **2005**, *109*, 5267–5272; d) B. Brena, Y. Luo, *J. Chem. Phys.* **2005**, *123*, 244305; e) D. L. Wang, H. T. Shen, H. M. Gu, Y. C. Zhai, *J. Mol. Struct.* **2006**, *779-800*, 47–51.
[12] a) X. F. Xu, Z. F. Shang, R. F. Li, Z. S. Cai, X. Z. Zhao, *J. Mol. Struct.* **2008**, *871-892*, 6–13; b) X. F. Xu, Z. F. Shang, R. F. Li, X. Z. Zhao, *Chem. J. Chin. Univ.* **2009**, *30*, 16–22.
[13] a) Q. B. Yan, Q. R. Zheng, G. Su, *Phys. Rev. B* **2006**, *123*, 165417; b) X. F. Xu, Y. M. Xing, X. Yang, J. C. Wang, Z. S. Cai, Z. F. Shang, Y. M. Pan, X. Z. Zhao, *Int. J. Quantum Chem.* **2005**, *101*, 160–168; c) X. F. Xu, Z. F. Shang, R. F. Li, Z. S. Cai, X. Z. Zhao, *J. Mol. Struct.* **2006**, *779-800*, 99–107; d) X. F. Xu, Z. F. Shang, R. F. Li, X. Z. Zhao, *Chem. J. Chin. Univ.* **2008**, *29*, 2413–2419; e) X. F. Xu, Z. F. Shang, R. F. Li, Z. S. Cai, X. Z. Zhao, *Phys. Chem. Chem. Phys.* **2009**, *11*, 8560–8569.
[14] L. L. Sun, Y. F. Chang, S. W. Tang, Z. L. Wang, R. S. Wang, *Mol. Phys.* **2008**, *106*, 1413–1418.
[15] a) L. Echegoyen, L. E. Echegoyen, *Acc. Chem. Res.* **1998**, *31*, 593–601; b) L. Dunsch, S. F. Yang, *Phys. Chem. Chem. Phys.* **2007**, *9*, 3067–3081.
[16] a) J. Y. Kim, K. Lee, N. E. Coates, D. Moses, T. Q. Nguyen, M. Dante, A. J. Heeger, *Science* **2007**, *317*, 222–225; b) R. B. Ross, C. M. Cardona, D. M. Guldi, S. G. Sankaranarayanan, M. O. Reese, N. Kopidakis, J. Peet, B. Walker, G. C. Bazan, E. V. Keuren, B. C. Holloway, M. Drees, *Nat. Mater.* **2009**, *8*, 208–212.
[17] a) H. W. Kroto, D. R. M. Walton, *Chem. Phys. Lett.* **1993**, *214*, 353–356; b) Z. J. Xu, W. Zhang, Z. Y. Zhu, J. G. Han, *Chem. Phys.* **2006**, *331*, 111–124; c) Z. J. Xu, J. G. Han, Z. Y. Zhu, W. Zhang, *J. Phys. Chem. A* **2007**, *111*, 656–665.
[18] a) Z. Y. Gao, W. S. Jiang, D. Sun, S. Y. Xie, R. B. Huang, L. S. Zheng, *Combust. Flame* **2010**, *157*, 966–969; b) Q. H. Weng, Q. He, T. Liu, H. Y. Huang, J. H. Chen, Z. Y. Gao, S. Y. Xie, X. Lu, R. B. Huang, L. S. Zheng, *J. Am. Chem. Soc.* **2010**, *132*, 15093–15095.
[19] W. Krätschmer, L. D. Lamb, K. Fostiropoulos, D. R. Huffman, *Nature* **1990**, *347*, 354–358.
[20] a) H. Murayama, S. Tomonoh, J. M. Alford, M. E. Karpuk, *Fullerenes Nanotubes Carbon Nanostruct.* **2005**, *12*, 1–9; b) H. Takehara, M. Fujiwara, M. Arikawa, M. D. Diener, J. M. Alford, *Carbon* **2005**, *43*, 311–319.

[21] X. Han, S. J. Zhou, Y. Z. Tan, X. Wu, F. Gao, Z. J. Liao, R. B. Huang, Y. Q. Feng, X. Lu, S. Y. Xie, L. S. Zheng, *Angew. Chem.* **2008**, *120*, 5420–5423; *Angew. Chem. Int. Ed.* **2008**, *47*, 5340–5343.
[22] a) P. Morvillo, *Sol. Energy Mater. Sol. Cells* **2009**, *93*,1827–1832; b) P. M. Allemand, A. Koch, F. Wudl, Y. Rubin, F. Diederich, M. M. Alvarez, S. J. Anz, R. L. Whetten, *J. Am. Chem. Soc.* **1991**, *113*, 1050–1051.
[23] T. F. Guarr, M. S. Meier, V. K. Vance, M. Klayton, *J. Am. Chem. Soc.* **1993**, *115*, 9862–9863.
[24] P. Boulas, F. D′Souza, C. C. Henderson, P. A. Cahill, M. T. Jones, K. M. Kadish, *J. Phys. Chem.* **1993**, *97*, 13435–13437.
[25] A. J. Bard, L. R. Faulkner, *Electrochemical Methods: Fundamentals and Applications*; Wiley, New York, **1980**.
[26] C. Jehoulet, Y. S. Obeng, Y. T. Kim, F. M. Zhou, A. J. Bard, *J. Am. Chem. Soc.* **1992**, *114*, 4237–4247.
[27] B. S. Sherigara, W. Kutner, F. D′Souza, *Electroanalysis* **2003**, *15*, 753–772.
[28] a) Y. Y. Liang, L. P. Yu, *Acc. Chem. Res.* **2010**, *43*, 1227–1236; b) Y. J. He and Y. F. Li, *Phys. Chem. Chem. Phys.* **2011**, *13*, 1970—1983 .
[29] a) J. B. Howard, J. T. McKinnon, Y. Makarovsky, A. L. Lafleur, M. E. Johnson, *Nature* **1991**, *352*, 139–141; b) J. B. Howard, J. T. McKinnon, M. E. Johnson, Y. Makarovsky, A. L. Lafleur, *J. Phys. Chem.* **1992**, *96*, 6657–6662; c) J. B. Howard, A. L. Lafleur, Y. Makarovsky, S. Mitra, C. J. Pope, T. K. Yadav, *Carbon* **1992**, *30*, 1183–1201.

Received: July 27, 2011
Revised: December 6, 2011
Published online: February 6, 2012

